Inter-joint coupling and joint angle synergies of human catching movements

Till Bockemühl, Nikolaus F. Troje, Volker Dürr

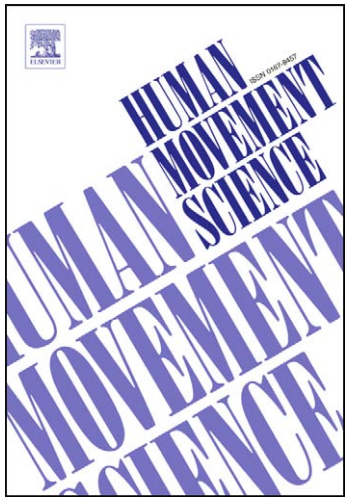

Inter-joint coupling and joint angle synergies of human catching movements

Till Bockemühl, Nikolaus F. Troje, Volker Dürr

PII: S0167-9457(09)00039-6
DOI: 10.1016/j.humov.2009.03.003
Reference: HUMOV 1148

To appear in: *Human Movement Science*

Please cite this article as: Bockemühl, T., Troje, N.F., Dürr, V., Inter-joint coupling and joint angle synergies of human catching movements, *Human Movement Science* (2009), doi: 10.1016/j.humov.2009.03.003

Inter-joint coupling and joint angle synergies of human catching movements

Till Bockemühl[1], Nikolaus F. Troje[2] and Volker Dürr[1]

[1]Dept. of Biological Cybernetics, University of Bielefeld, PO Box 10 01 31, 33501 Bielefeld, Germany

[2]Dept. of Psychology, Ruhr-University, 44780 Bochum, Germany

Corresponding author:
Till Bockemühl, Dept. of Biological Cybernetics, University of Bielefeld, PO Box 10 01 31, 33501 Bielefeld, Germany
Email: till.bockemuehl@uni-bielefeld.de
Phone: +49-521-106 5519
Fax: +49-521-106 89010

Keywords: motor coordination; perceptual motor processes; multivariate analysis; grasping; posture

PsycINFO classification: 2330 (Motor Processes)

Abstract

A central question in motor control is how the central nervous system (CNS) deals with redundant degrees of freedom (DoFs) inherent in the musculoskeletal system. One way to simplify control of a redundant system is to combine several DoFs into synergies. In reaching movements of the human arm, redundancy occurs at the kinematic level because there are an unlimited number of arm postures for each position of the hand. Redundancy also occurs at the level of muscle forces because each arm posture can be maintained by a set of muscle activation patterns. Both postural and force-related motor synergies may contribute to simplify the control problem. The present study analyzes the kinematic complexity of natural, unrestrained human arm movements, and detects the amount of kinematic synergy in a vast variety of arm postures. We have measured inter-joint coupling of the human arm and shoulder girdle during fast, unrestrained and untrained catching movements. Participants were asked to catch a ball launched towards them on 16 different trajectories. These had to be reached from two different initial positions. Movement of the right arm was recorded using optical motion capture and was transformed into 10 joint angle time courses, corresponding to 3 DoFs of the shoulder girdle and 7 of the arm. The resulting time series of the arm postures were analyzed by Principal Components Analysis (PCA). We found that the first three principal components (PCs) always captured more than 97% of the variance. Furthermore, subspaces spanned by PC sets associated with different catching positions varied smoothly across the arm's workspace. When we pooled complete sets of movements, three PCs, the theoretical minimum for reaching in 3D space, were sufficient to explain 80% of the data's variance. We assumed that the linearly correlated DoFs of each significant PC represent cardinal joint angle synergies, and showed that catching movements towards a multitude of targets in the arm's workspace can be generated efficiently by linear combinations of three of such synergies. The contribution of each synergy changed during a single catching movement and often varied systematically with target location. We conclude that unrestrained, one-handed catching movements are dominated by strong kinematic couplings between the joints that reduce the kinematic complexity of the human arm and shoulder girdle to three non-redundant DoFs.

1. Introduction

Reaching for a target located in peripersonal space is a task that most of us conduct many times each day. There is a general consensus that the control of such aimed limb movements requires a series of sensorimotor transformations, which map the target's retinal image onto an appropriate muscle activation pattern that in turn moves the limb towards the target (Beek, Dessing, Peper & Bullock, 2003; Georgopoulos, 1991; Kalaska & Crammond, 1992; Wolpert & Ghahramani, 2000). Several of the steps in this series of transformations involve one-to-many mappings, which complicate the necessary computations. This issue is known as the redundancy problem (Bernstein, 1967).

An example for the redundancy problem is the transformation of a desired hand position into an appropriate arm posture. Finding unambiguous solutions for this transformation is not a trivial task. The CNS overcomes this problem routinely and often generates reproducible behavior that exhibits invariant parameters, which have been observed in classical studies such as Soechting and Lacquaniti (1981), Atkeson and Hollerbach (1985), Morasso (1981), and Flash and Hogan (1985). The results of these studies imply additional constraints that are realized within the nervous system and have led to the formulation of a range of hypotheses concerning the generation of goal-directed limb movements. One influential idea in motor research is the concept of motor primitives and movement synergies (Bernstein, 1967; Lee, 1984; Macpherson, 1991, for a recent review, see Ting and McKay, 2007). This concept assumes that the various degrees of freedom (DoFs) of a motor system are not controlled independently but instead are coupled in their actions. In theory, this would lead to a reduction of the effective number of DoFs to a level that can be controlled more easily by the CNS.

There are numerous studies suggesting that the coupling of DoFs occurs on various stages. These stages encompass the simultaneous activity of several muscles acting on one joint (Haruno & Wolpert, 2005), multi-joint synergies (Debicki & Gribble, 2005; Gottlieb, Song, Hong, Almeida, & Corcos, 1996; Latash, Aruin, & Shapiro, 1995; Santello, Flanders, & Soechting, 1998; Yang, Zhang, Huang & Jin, 2002) or the combination of basic behavioral modules (Bizzi, 2003; d'Avella & Bizzi, 2005; d'Avella, Saltiel, & Mussa-Ivaldi, Giszter, & Bizzi, 1994; Sanger, 2000). Although several

mathematical methods are suitable for detecting synergies, some of which exhibit even better performance than Principal Component Analysis (Tresch, Cheung, & d'Avella, 2006), PCA is a common tool in the analysis of motor behavior and often reveals evidence of fundamental building blocks of the studied movements (Daffertshofer, Lamoth, Meijer, & Beek, 2004). One advantage of PCA is that it captures covarying and, thus, coupled DoFs in a very intuitive manner. An important second reason for the use of PCA in the study presented here was that PCA only considers linear correlations among DoFs which can be considered as the most-simple, i.e., minimal model of inter-joint coupling. This minimal model can be of great relevance to studies in computational neuroscience, as it determines to what extent the natural complexity can be explained by a linear approach.

Studies that apply PCA to biological movement data have focused on a wide variety of movements, including the formation of hand postures (Santello, Flanders, & Soechting, 1998), drawing tasks (Sanger, 2000), gender identification based on gait (Troje, 2002), leg wiping reflexes in the frog (d'Avella & Bizzi, 1998), and inter-limb coordination (Forner-Cordero, Levin, Li, & Swinnen, 2005). Generally, these studies argue in favor of a modular organization of the CNS because they succeed in describing the observed physiological complexity by means of a small number of PCs. In the context of human arm movements, PCA has been applied to the analysis of rhythmic juggling movements (Post, Daffertshofer, & Beek, 2000), object retrieval (Sabatini, 2002), and whole body reaching movements (Thomas, Corcos, & Hasan, 2005). Many studies use a setup related to the common “center-out task” (Galloway & Koshland, 2002; Gomi & Kawato, 1997; Morasso, 1981), in which participants are instructed to execute relatively slow, well-planned pointing or reach-to-grasp movements constrained to a horizontal plane. Sabatini (2002) found that such planar movements are effected by two types of muscle activity patterns, one for the outward and one for the inward part of the movement. In spite of its experimental benefits, the center-out task, for the most part, neglects the natural dexterity of the human arm that is a result of 10 DoFs: three in the shoulder girdle, three in the shoulder joint, two in the elbow and lower arm, and a further two in the hand joint. To date, it is an open question how these 10 DoFs are coupled to each other when the arm is mechanically unrestrained. Arbitrary positioning and orientation of the hand in space requires three DoFs of translation for positioning (along the axes x, y,

z) and further three DoFs of rotation for orientation of the inner hand surface (roll, pitch, yaw). Since humans are able to attain voluntarily many different hand orientations at any given hand position, it is plausible to assume that at least six DoFs must be used if all behavioral tasks of a human arm were considered. However, some behavioral tasks could require less than six DoFs, for example if hand orientation varied systematically with hand position.

To date, PCA studies on unrestrained arm movements have been either limited to the sagittal body plane (Thomas, Corcos, & Hasan, 2005) or to the trajectories of manipulated objects (Post et al., 2000). Thus, the effective redundancy of natural human reaching movements has never been determined. In particular, it is unknown how the coupling of DoFs might be modulated depending on the location of the target in the arm's workspace.

The goal of our study was to elicit fast and unrestrained reaching movements in a large part of the 3D workspace of the arm, involving the intuitive and natural use of a large number of joints. Catching movements meet these criteria well, as most people have a natural aptitude for catching and, as opposed to juggling (Post et al., 2000), do not require extensive training sessions. Although participants can accomplish a catching task reliably, it requires a considerable amount of attention, which ensures that participants concentrate on the task. This facilitates natural and fast movements, while conscious planning is minimized.

Catching movements are a well-studied paradigm in the study of interceptive actions. They definitely require the use of three translational DoFs for hand positioning in space but it is unclear to what extent additional DoFs are required to account for hand orientation. Several studies have addressed the problem of visual extraction/prediction of the future catching position (Alderson, Sully, & Sully, 1974; Peper, Bootsma, Mestre & Bakker, 1994; Montagne, Laurent, Durey & Bootsma, 1999), or the impact of spatio-temporal constraints imposed by the balls flight direction and speed (Laurent, Montagne, & Savelsbergh, 1994; Mazyn, Montagne, Savelsbergh, & Lenoir, 2006). The latter studies revealed that acceleration and deceleration phases of the hand movement depend on the speed of the ball and, thus, time to contact. Based on the experimental evidence on spatio-temporal constraints and timing of human catching movements, Beek et al. (2003) proposed to model them as prospective movements with continuous

adjustment of hand speed and direction by means of a feedback controller. Whereas it is clear that a feedback controller would account for the appropriate timing of the movement, a major question concerns how a controller could deal with the redundancy problem posed by the 10 DoFs of the arm and shoulder girdle. Recently, cross-correlations of synchronously recorded joint angle time courses revealed that at least some output variables of the neural controller are significantly coupled during catching (Mazyn, Montagne, Savelsbergh, & Lenoir, 2006). The present study takes a step further and measures the amount of coupling among all 10 DoFs of the human arm and shoulder girdle. It does so for catching movements that traverse a wide range of arm postures.

The main objective of the present study was to identify joint angle synergies within the physiological joint angle space of the human arm and shoulder girdle. To this end, we applied PCA to determine the amount of inter-joint coupling and the number of effective DoFs underlying human catching movements that involve a 10D joint angle space. We reasoned that, if a small set of principal components would exist that allowed for the description of at least 95% of the variance within this space, these principal components would capture the synchronous movement of several joints and, hence, could be interpreted as joint angle synergies. The less joint angle synergies would be necessary for posture reconstruction, the more the dimensionality of the control problem could be reduced.

We show that three PCs are generally sufficient to describe more than 97% of variance within the 10D posture space of single catching movements. The contribution of individual PCs depends systematically on target location. Finally, we use PCs to reconstruct arm postures and derive arm movements. Based on these findings, we argue that PCs not only provide a tool for analyzing biological movement but also are a candidate format for joint angle synergies that could contribute to reducing the dimensionality of joint angle motor space.

2. Methods

2.1. Participants

In total, nine subjects (seven males, two females) participated in the experiments. Their age ranged from 21 to 34 years. Eight of the participants were naïve as to the scientific background of the study. All participants were right-handed, had normal or corrected-to-normal vision, and had no obvious or known motor deficits. Participants gave their informed consent to the experimental procedures carried out within the scope of the study.

2.2. Experimental procedure

Participants were seated comfortably on a chair in the center of the experimental setup. A custom-made shooting device attached to a tripod was placed in front of the participant at a distance of 280 cm. A table-tennis ball could be launched manually from the shooting device onto 16 different trajectories traversing the workspace of the participant's right arm (Fig. 1a). These trajectories were the same for all participants and were not adjusted with respect to individual differences in body size or arm lengths. The velocity of the ball ranged from 5.0 to 5.3 m/s. This corresponds to a flight time range between 530 and 560 ms, assuming 280 cm as the length of the ball's flight trajectory. (For the sake of optimal spatial resolution of the joint angle measurements, the flight trajectory could not be tracked in its entirety.)

To elicit goal-directed arm movements we instructed the participants to catch the approaching ball at a convenient point on its flight path. Since we wanted the behavior to be as natural as possible, no specific instructions were given with respect to movement speed, the catching point, or how to catch the ball. Participants were encouraged to move only their right arm, but there were no physical constraints or instructions to restrain movements of the trunk. Prior to the actual experiment participants were familiarized with the setup and the procedure.

(Fig. 1 approximately here)

For each trial, participants had to adopt one of two predefined initial postures. In initial posture one, the right arm of the participant hung in a relaxed posture besides the participant's torso. In initial posture two, the right hand rested on the participant's right thigh (Fig. 1a). Idealized target positions are indicated by grey circles and each ball trajectory determined one possible target position. Lateral variations of the ball's flight trajectory were brought about by shifting the position of the tripod along a base line parallel to the participant's frontal plane. Vertical variations were achieved by altering the angle of the shooting device (Fig. 1b). Each experimental session consisted of two subsessions. Within one subsession, there were 16 blocks of at least three trials, each consisting of one movement. In each block, the ball was launched onto one of the 16 predefined trajectories once. The order of blocks, i.e., target positions, was randomized. In subsession 1, the first movement within a block started from initial arm position 1, the second movement started from initial position 2, and the third movement started from initial position 1 again (succession of 1-2-1). Subsession 2 was comprised of another random sequence of the sixteen different trajectories. Here, the within-block succession of initial positions was 2-1-2. Each movement was repeated at least twice. If a movement was not successful, it was repeated from the same initial position until it was successful. However, error trials (i.e., ball missed entirely) were so rare that they were discarded. Overall, individuals completed between 6 and 9 successful trials per start-target combination.

2.3. Motion Capture

Kinematic data were recorded using an optical motion capture system (Vicon Motion Systems, Oxford, UK) consisting of 9 high-speed CCD cameras with 120 Hz temporal and approximately 1 mm of spatial resolution. Thirteen spherical retroreflective markers (diameter 14 mm) were attached to the participants' skin using double-sided adhesive tape. Markers were positioned on easily identifiable bony landmarks (Fig. 2). The table-tennis ball was also covered in retroreflective foil. The setup provided Cartesian coordinates of all marker positions and of the ball.

(Fig. 2 approximately here)

2.4. Kinematic model

For the kinematic analysis, we modeled the arm as a kinematic chain with 4 segments articulated by four joints and 10 DoFs in total. This chain originated at the upper sternum marker which also served as the origin of the body-fixed coordinate system. From proximal to distal, the kinematic chain consisted of a collarbone segment with three DoFs, an upper arm segment with three DoFs, a lower arm segment with two DoFs and a hand segment with two DoFs (Fig. 2). Prior to the actual experiment participants executed calibrating movements that consisted of the successive movements of all DoFs of the arm. Based on these data, we determined segment lengths, the joint centers of the shoulder, elbow, and wrist, and the position of the markers relative to the segments they were attached to. This was done for each participant individually.

2.5. Joint angles

To calculate joint angles of a particular posture we used forward kinematics of the arm model described above. Using nonlinear optimization routines based on the Levenberg-Marquardt algorithm (Levenberg, 1944; Marquardt, 1963) of MATLAB 7 (The MathWorks) we adapted the joint angles of the arm model such that the sum of squared distances between model markers and their real counterparts was minimal. Thus, we were able to determine joint angles based on kinematic models of nine individual participants. The optimization was done for all movements in a frame-by-frame manner. Although our models simplified the true arm kinematics, both by neglecting skin movements and by keeping the centers of rotations of all joints fixed relative to the segments, the matching error was sufficiently low. Median marker mismatch was 8.3 mm per marker (25th percentile: 6.7 mm, 75th percentile: 10.2 mm), which amounted to 60% of the markers' diameter. The onset of a trial was defined as the time when hand velocity exceeded 0.2 m/s (1.6 mm per frame). Termination of a movement was defined as the time of hand contact with the ball which, in turn, was determined by visual inspection of the motion capture data.

In order to achieve equal weighting of all start-target combinations and to obtain data sets of equal size for all participants, we decided to average trials for each start-target combination and participant. To allow for averaging of arm movements, each trial was normalized to 100 single postures by spline interpolation. Duration of arm movements

varied between 300 ms to 700 ms (median: 391 ms, percentiles: 25% = 350 ms, 75% = 441 ms). This range can be explained by different distances between starting and catching position of the hand. Catching positions on the contralateral side were further away and took longer to reach than those on the ipsilateral side. In total, we obtained 32 average movements per participant (2 initial positions x 16 target positions). All further analyses were carried out on these average time courses (except supplementary Figs. S2b, S3, S4, and S5). We controlled for a potentially biasing effect of averaging by comparing the results with an analysis that was based on all single trials (see Section 3.4). Averaging introduced no significant bias into our analysis.

2.6. PCA

PCA describes the distribution of variance of the underlying data set by vectors or principal components. PCs thereby constitute a new orthonormal coordinate system whose unity vectors are aligned with the directions of largest variance. Although the number of PCs is equal to the number of variables often only the first few components are needed to capture most of the variance in a data set (see also Manly, 2004). Computing PCA is identical to finding the eigenvectors and eigenvalues of the data set's covariance matrix or correlation matrix. In our case, the correlation matrix was used in order to attribute equal weight to each observed variable. Otherwise, large absolute values of variables might have dominated the result of the PCA. To achieve such equal weighting, the covariance matrix is scaled, separately for each component, by the variances of the respective pair of observation variables. Mathematically, this is identical to carrying out the PCA on the correlation matrix of the original data set instead of the covariance matrix. Equation 1 shows the correlation measure used in this study, where *a* and *b* represent a pair of observation variables, $\bar{a}$ and $\bar{b}$ are their respective means, and *n* is the number of observations.

$$CORR(a,b) = \frac{COV(a,b)}{SD(a) \cdot SD(b)} = \frac{\frac{1}{n}\sum_i \left(a_i - \bar{a}\right) \cdot \left(b_i - \bar{b}\right)}{\sqrt{\frac{1}{n}\sum_i \left(a_i - \bar{a}\right)^2} \cdot \sqrt{\frac{1}{n}\sum_i \left(b_i - \bar{b}\right)^2}} \quad \text{(Eq. 1)}$$

All necessary calculations were done using MATLAB 7 (The MathWorks). We carried out PCA on sets of 10-dimensional postures, each of which constitute a point in joint

angle space. Each PCA yielded a set of 10 PCs and corresponding eigenvalues. The PCs of a set of postures thereby satisfy the criterion

$$\vec{p} = \vec{p}_m + \sum_{i=1}^{n} c_i \vec{p}_i \qquad \text{(Eq. 2)},$$

where *n* PCs, $\vec{p}_i$, can be weighted by their respective scores, c_i, and added to the mean posture vector, $\vec{p}_m$, such that the result equals any recorded arm posture, $\vec{p}$. The underlying rationale of this analysis is the idea that if two or more joint angles were coupled, such that they would always move in synchrony and in a fixed magnitude ratio, this would result in significant linear correlation of these coupled joint angles. PCA would detect these linear correlations and sort them according to the fraction of variance that they explain. As a result, the loadings of each $\vec{p}_i$ in Eq. 2 represent a set of 10 joint angles that are always scaled together whenever the posture of the arm and shoulder girdle changes. This combined scaling reflects inter-joint coupling and can be interpreted as a sign of synergy.

In practice, we applied PCA in two ways. First, we computed PCA separately for each averaged angular time course of all 32 start-target combinations which were coded as matrices of 100 postures x 10 angles each. This analysis will be referred to as single-target-PCA. Then we pooled average movements associated with one initial arm position of single participants. Thus, the analyzed data consisted of a matrix with 1600 postures x 10 joint angles per person and start position. This analysis based on sets of 16 movements will be referred to as multiple-target-PCA.

In order to determine the minimal number of PCs that are sufficient to reconstruct most of the observed arm postures, we applied two criteria. First, we omitted those PCs whose eigenvalues were smaller than one because such PCs would explain less variance than one variable of the original data set (Kaiser-Guttman criterion; see Jackson, 1993). In our case, this corresponded to a minimum explained variance of 10%. The second criterion was that, ideally, at least 95% of the total variance should be explained. Since these two criteria could potentially lead to different numbers of PCs (e.g., if three PCs explain 90% of the variance, a fourth one can only explain less than 10% but is required to reach the 95% threshold) we also applied a bootstrap Kaiser-Guttman criterion (e.g., Jackson, 1993) in case of the multi-target PCA. Finally, we

always considered at least three PCs because this is equal to the minimal number of PCs that is necessary to explain arbitrary hand positions in 3D-space (for further explanation see results Section 3.1).

Note that the performance of PCA in reducing data dimensionality and the significance of single PCs is expressed by the fraction of data variance explained. In our case, the term data variance refers to the dimensionless total variance within the 10D posture space after normalization of each joint angle to unit variance (see Eq.1). It does not refer to the variance of a joint angle or the covariance between two joint angles, both of which would be measured in degrees.

2.7. Comparison of PC subspaces

It should be noted that, in contrast to many other studies that apply PCA, all items of our data vectors are joint angles and, thus, their magnitudes are immediately comparable with each other. As a consequence, it is possible to define a metric that allows to measure distances within the original 10D joint angles space. For example, the set of PCs that accounts for most of the variance, say 95%, of a particular movement spans a low-dimensional subspace within 10D joint angle space. As a metric to quantify the similarity of different PCA results, we compared PC subspaces spanned by three PCs (see also Fig. 5 for results). We calculated the distance between two such subspaces according to

$$dist(U,V) = \sin(\varphi) = \sqrt{1 - s_{\min}{}^2(U^T V)} \qquad \text{(Eq. 3)}.$$

U and *V* are 10 x 3 matrices that each contain three PCs (i.e., represent two distinct PCAs) as column vectors. They define the subspaces. The column vectors of *U* and *V* are normalized to unit length 1. Because, by definition, PCs are orthogonal to each other, *U* and *V* are orthonormal matrices and their column vectors span a 3D subspace within 10D joint angle space. The distance between these subspaces, *dist(U,V)*, is defined by the smallest angle *φ* by which *U* can be rotated to match *V*. *sin(φ)* is estimated numerically by finding the minimal singular value s_{min} of the matrix $U^T V$, which is a 3 x 3 matrix that contains dot products of all pairs of PCs from *U* and *V*. For details on singular value decomposition see Golub and van Loan (1989). Thus, Eq. 3 is the matrix version of the calculation of the smallest angle between two vectors, where the cosine of the angle is equal to the dot product of the normalized vectors. The angle

φ in Eq. 3 describes the similarity of the subspaces *U* and *V*, with 0° indicating identity and 90° indicating orthogonality. A mean value of 81° indicates chance level similarity for 3D subspaces within a 10D space.

2.8. Reconstruction of movements

A reduced set of PCs can be used to approximate the original data. While this entails a loss of accuracy, the loss will be relatively small if the used PCs capture a large amount of variance. Using Eq. 2 with $n = 3$ we can approximate a posture by neglecting the amount of variance accounted for by higher PCs. The scores c_1 to c_3 can be found by projecting $\vec{p}$ onto the respective PC $\vec{p}_i$. As PCs and the mean posture stay constant for one data set, we can then describe a given movement exclusively by the time courses of the three scores c_1 to c_3.

3. Results

3.1. Hand trajectories

As our analysis of inter-joint coupling and movement synergies in the arm and shoulder-girdle is entirely based on joint angles, all computations were carried out on vectors containing 10 joint angles, or on time courses thereof. To provide an intuitive demonstration of what the actual catching movements looked like, Fig. 3 shows representative hand trajectories of one participant. Trajectories were always curved and, in the course of the entire experiment, the hand traversed a 3D volume with the approximate size of 800 mm by 400 mm by 800 mm (x, y, and z, respectively). Standard deviations of different target positions were smaller than the width of a human hand (i.e., < 100 mm) and did not overlap. The idealized arrangement of target positions shown in Fig. 1b can be recognized clearly in Fig. 3. Because we did not scale the setup according to the participants' size or arm lengths, preferred catching positions differed by 57 to 145 mm among participants (standard deviation for average catching positions of all participants). Catching locations were always spaced evenly (compare Figs. 1b and 3). Irrespective of their body size, all participants had to cover a large portion of their arm's workspace (arm lengths were 59 cm to 74 mm, distance from shoulder center to palm) and the arm was often nearly stretched out when catching balls at target positions 1, 4, and 16).

(Fig. 3 approximately here)

Note that all trajectories in Fig. 3 are curved and trajectories toward different target positions span a 3D volume. As a consequence, at least three PCs are required to explain all trajectories. The reason for this is that each PC describes a linear combination of joint angles that allow displacement of the hand along a single curved, albeit 1D trajectory. Two PCs will allow displacement along a curved, but at most 2D surface. To move the hand away from this surface, at least one further, third PC must be postulated to explain all trajectories shown in Fig. 3.

At least three DoFs of movement are required to position the hand at an arbitrary position in a 3D volume. The complete set of recorded catching movements does span a 3D volume because both starting points lay well outside the plane spanned by the target positions (or, considering the spread of catching positions, even well outside the subspace that includes all catching positions). Suppose that the 10 DoFs of the arm and shoulder girdle were found to correlate so substantially that a PCA could group them into a small number of joint angle synergies. Then, each synergy would couple a set of joint angles into a single DoF. Since PCs are mutually orthogonal (by definition) and, therefore, independent from each other, three synergies are needed to obtain three DoFs. Thus, no less than three PCs can capture all arm postures recorded in our experiments.

3.2. Single-target-PCA

With the single-target-PCA for all participants and all data sets, three PCs were always sufficient to capture more than 97% of the data's variance. This was true for data sets associated with either initial position (Fig. 4). In all cases, the first PC accounted for at least 68% of the variance. In several cases this value reached 75%. The remaining variance could almost completely be explained by the second and third PC. On average, these PCs accounted for 20% (min. 13%, max. 26%) and 5% (min. 2%, max. 7%) of the variance, respectively.

Note that the ata were not pooled across participants, mainly because participants differed in the size, weight, and muscle force of their arms. Therefore, one set of joint angles would correspond to different arm postures, joint torques, and associated muscle activations in different participants. As yet, Fig. 4 shows that PCA reduces the number of effective DoFs in all participants and the relative contributions of the three PCs are very similar across participants.

In conclusion, the results indicate strong kinematic couplings between individual joints in the arm and shoulder girdle and, therefore, high redundancy in the underlying data sets. The first three PCs are necessary to satisfy the 95% variance criterion (see Section 2.6), whereas the third PC contributes less than the 10% variance required by the Kaiser-Guttman criterion. According to the latter criterion, trajectories of individual start-target combinations could be described reasonably well by only two effective DoFs. Nevertheless, our considerations outlined in the preceding Section 3.1 led us to consider always at least three PCs.

(Fig. 4 approximately here)

3.3. Comparison of subspaces

Considering that three PCs are sufficient to describe single-target data sets, it was necessary to evaluate the similarity of these solutions, in particular with respect to target position. In principle, we could have obtained specialized solutions for individual start-target combinations. To identify any systematic trend across our solutions we determined the similarity between subspaces spanned by sets of three PCs associated with adjacent target positions. For this, we selected two series of target positions. The first series formed a horizontal transect across the arm's workspace including target positions 2, 6, 10, 13, and 15 (Fig. 5a). The second series formed a vertical transect including target positions 5 to 8 (Fig. 5b). For both series we calculated the similarity of each pair of subspaces. This was done separately for each participant. We found that the similarity between each pair of subspaces was significantly higher than expected for random placement ($p < .01$ for initial position 1, $p < .02$ for initial position 2, Bonferroni-corrected for multiple comparisons). Moreover, distance between subspaces generally depended on the spatial distance between target positions. The closer the target

positions were, the more similar were their associated PC subspaces. For example, distance values of the subspace for the most contralateral target 15 systematically increased when compared with increasingly ipsilateral targets at the same height (Fig. 5a). Similarly, distance values of the subspace for the highest target 5 in Fig. 5b systematically increased when compared with lower targets (Fig. 5b). This effect was more pronounced in subspaces of the horizontal transect (Fig. 5a) than in those of the vertical transect (Fig. 5b). The only target for which there was no systematic difference of its own PC subspace and those of its adjacent targets was the low target 8 that was located close to the ipsilateral knee of the participants.

(Fig. 5 approximately here)

3.4. Multiple-target-PCA

As the similarity analysis indicated a close relationship between neighboring PC sets, we examined whether different movements could be described by a single set of more general PCs with similar quality. For this, we computed multiple-target-PCA for both initial positions and each participant separately (Fig. 6). Analogous to single-target-PCA, we found that three PCs were sufficient to capture a large portion of the data's variance. Cumulative values for three PCs varied over participants from 78% to 91% and the first PC captured between 37% and 57% of the data's variance. Thus, the first PC captured a smaller fraction of the variance than in single-target-PCA, whereas the second and third PCs played much larger roles, with fractions of explained variance ranging from 19% to 30% for the second PC and from 10% to 17% for the third PC. Thus, according to the 95% criterion, further PCs would have to be considered, however no additional PCs would have satisfied the Kaiser-Guttmann criterion. To assess validity of our selection of three PCs, we also applied a bootstrap method to quantify the variance of our PCA. The results are listed in Table 1, showing that the variance of the bootstrapped eigenvalues is always less than 1%. Mean values are nearly identical with those shown in Fig. 6. The small variance shows that the first three PCs always indicate significant inter-joint coupling.

(Fig. 6 approximately here)

(Table 1 approximately here)

Finally, we tested whether normalization of the joint angle ranges to unit variance could have lead to an overrating of the smallest PC. For this, we re-calculated both the single-target and multiple-target-PCA for the covariance matrices instead of the correlation matrices (see method Section 2.6 and Eq. 1). Comparison of the results with those shown in Figs. 4 and 6 reveals that both procedures succeed in capturing most of the data's variance with two or three PCs and that at least three PCs are necessary to explain movements to more than one target (Supplementary Figs. S1 and S2a). The same holds true when trials were not averaged per participant and start-target combination, but all single trials were included (Supplementary Fig. S2b).

3.5. Time course of scores

Since our multiple-target-PCA used a single set of PCs for all movements, different movements solely differ in the time courses of their respective scores (see Eq. 2). Therefore, we examined whether features of these time courses, such as the maximum magnitude or the timing of local peaks, could be related to the spatial properties of the respective hand movements. For this purpose we chose the same horizontal and vertical series of target positions as in Fig. 5. For each of these movements, we solved Eq. 2 for c_1 to c_3, i.e., the scores associated with the first three PCs. As the arm posture $\vec{p}$ changes over the course of the catching movement, the scores c_1 to c_3 change as well. Fig. 7a shows the results for the horizontal series of target positions; Fig. 7b shows the results for the vertical series. Scores at time 0 represent the initial arm posture.

The scores' time courses deviated from each other in a systematic manner, revealing specific contributions of individual PCs to movement into a particular direction. For example, the peak magnitude of the score of PC 2 in Fig. 7a systematically decreased when horizontal target positions shifted from ipsilateral (pos. 2 and 6) to contralateral (pos. 13 and 15). A similar dependence was found for the score of PC 3 of the same set of movements, yet the timing of the local minima differed. Target-dependent divergence of the time courses was strongest at the end of the movement for PC 2, and shortly after

half-time for PC 3 (Fig. 7a). Moreover, divergence of scores decreased again for PC 3. Depending on the horizontal target position, the time course formed a trough that was most pronounced when the target position was contralateral to the catching arm.

PC 3 also strongly contributes to the vertical target displacement along the transect through positions 5 to 8 (Fig. 7b). However, in contrast to its effect on horizontal target displacement, divergence begins later and steadily increases until the end of movement. At the end of the trajectory, large scores of PC 3 correspond to high target positions within the arm's workspace. In conclusion, the relative contribution of a given PC to catching movements not only depends on target position, but can also vary over time in a non-monotonic manner.

(Fig. 7 approximately here)

In order to assess how the magnitude of the gaps between the time courses in Fig. 7 relate to the variability of each time course, we estimated the effect of PC variability on the spread of each time course. For this we applied a bootstrap analysis in which we sampled 50 random sets of postures from the multiple-target data set and calculated corresponding sets of PCs and time courses. The result showed that the gaps between time courses for movements to different targets were often larger than the variance among the 50 bootstrap solutions (Supplementary material, Fig. S3). Much like in Fig. 7, all three PCs varied in importance during a catch, and did not vary uniformly. Although the spread within each group of corresponding time courses differed over time, the systematic dependence on target location remained clear, although there was increased overlap where time courses in Fig. 7 were close to each other (e.g., PC 3 in Fig. 7a and PC 2 in Fig. 7b, both toward the end of the movement).

3.6. Reconstruction of movements

A small number of PCs is adequate to describe the movements analyzed here. To test the quality of this description, we reconstructed joint angle time courses using the first three PCs only, obtained either from single-target-PCA or from multiple-target-PCA. Fig. 8 shows a representative example based on multiple-target-PCA. Several joint angle time courses were reconstructed with very high accuracy, for instance the angles

clavicula θ and φ, humerus θ and ψ, and hand φ. Other reconstructed time courses showed more pronounced deviation from the original, for example the angles ulna θ, ulna ψ, and hand θ. However, the qualitative characteristics of all original time courses were well-preserved. Importantly, reconstruction from the reduced set of PCs never led to unphysiological joint angles. This indicates that the inter-joint couplings captured by any one of the first three PCs never violate physiological boundaries and, therefore, qualify as joint-angle synergies that correspond to coordinated changes in posture. To determine the effect of inter-trial variability on the quality of this reconstruction, we re-calculated all joint angle time courses on the basis of the 50 bootstrap solutions of the PCA (same bootstrap analysis as described in the previous section). The result shows that a random sample of postures causes only little variability among the reconstructed time courses (Supplementary material, Fig. S4). Moreover, the bootstrapped PCs do not introduce unphysiological joint angles into the reconstructed time courses, indicating that inter-trial variability does not confound the physiological plausibility of the extracted joint angle synergies.

(Fig. 8 approximately here)

To assess the accuracy of reconstruction more quantitatively we first computed hand trajectories using forward kinematics based on reconstructed angular time courses. We then compared reconstructed hand trajectories and original hand trajectories via root mean squared error (RMSE). This was done for trajectories based on both single- and multiple-target-PCA. Generally, the RMSE for reconstruction based on single-target-PCA was low, indicating high accuracy with a median of 11.7 mm and maximum deviation never exceeding 50 mm. For the results based on multiple-target-PCA, however, the RMSE reveals lower accuracy. Here, the median was 63.3 mm with maximum errors up to 140 mm. In both cases, median errors are well below the width of the human hand, and small compared to the considered workspace (approximately 0.7 m^2 cross-sectional area at catching distance).

3.7. Features of PCs

In order to illustrate the effect of inter-joint coupling captured by individual PCs, we generated three artificial movements. Each one of these was based on only one of the first three PCs of a representative participant as obtained from multiple-target-PCA. We modulated each PC's score sinusoidally around the average arm posture with maximum score amplitude set to three standard deviations (with respect to the SD of the score distribution of the original data set). As a result, the movement amplitude fell within the range observed during the experiments. Videos of these movements were provided in the supplementary material.

The movement expressed by PC 1 is an upward rotation of the arm, accompanied by an adduction of the shoulder girdle. The resulting movement is reminiscent of the gesture we make when raising a sign for a vis-à-vis observer to see. The movement expressed by PC 2 is an inward and forward movement of the hand, with an elbow extension accompanying the adduction of the upper arm. It resembles a pushing movement along an oblique line. The movement expressed by PC 3 is an upward and lateral movement of the slightly extended arm, with very little movement of the elbow.

(Fig. 9 approximately here)

In addition, Fig. 9 shows the magnitude of inter-joint coupling as captured by the first three PCs. The loadings of each PC are shown for four different situations. PC 1, which captures most of the data's variance, turns out to be very similar across different situations presented here. This shows that PC 1 is robust against changes in start posture and calculation method. Therefore, it must represent more general movement features. As judged by the grade of similarity among the four situations shown in Fig. 9, these general movement features are governed by levation and protraction of the shoulder girdle (shoulder θ and φ), inward rotation of the upper arm (humerus φ), pronation of the lower arm (ulna ψ) and both hand angles. While PCs 2 and 3 still retain common elements they differ more strongly between situations and might be responsible for situation-specific features of movements.

In order to assess the robustness of the PC loadings shown in Fig. 9, and in addition to the bootstrap analysis presented in the three previous sections, we calculated a second

error estimate that assessed the potential effect of marker mismatch in our motion capture procedure. For this we determined the effect of added noise to the recorded marker positions (standard deviation of noise was 8 mm, compared to 8.3 mm median marker mismatch as described in Section 2.5). The resulting mean PC loadings were very similar to those of the original data set (see supplementary figure S5). Loadings of the first PC varied very little in the presence of noise, with coefficients of variation ranging between .03 and .37. In the second and third PC, sensitivity to noise was more pronounced and coefficients of variation were larger than 1 in four out of ten loadings, but for a mutually different subset of loadings in the two PCs. In conclusion, the effects of both error sensitivity (Fig. S5) and situation-specific variability (Fig. 9) increase the variability of the PC loadings with decreasing importance of the PC. However, the number of joint angle synergies that describe most of the variance in the experimental data remains unaffected, and the overall pattern of these joint angle synergies varies only moderately for a single participant.

4. Discussion

In this study we showed that 10D joint angle kinematics of mechanically unrestrained catching movements in humans can be efficiently characterized by the linear combination of as few as three PCs. This was the case for both single-target-PCA (Fig. 4) and multiple-target-PCA (Fig. 6). Given the fact that we analyzed 3D arm movements with hand positions covering a substantial 3D volume, finding three PCs is equivalent to finding the theoretical minimum number of components. In fact, the result suggest that the six DoFs for arbitrary hand positioning (translation along three axes) and orientation (roll, pitch and yaw rotation) are not required in unrestrained, one-handed catching.

In single-target-PCA, the orientation of subspaces spanned by three PCs tends to vary systematically across the arm's workspace (Fig. 5). In multiple-target-PCA, target positions are encoded via the time courses of PC scores. Individual PCs thereby contribute to shifts in particular directions within the arm's workspace (Fig. 7). The reconstruction of original movements is very accurate when based on the first three PCs of that very movement, but accuracy declines from 11.7 mm to 63.3 mm (RMSE) if PCA is based on an entire set of movements. Finally, since translation movements of the

hand occur along all three axes, linear reconstruction with three PCs implies that there can be only one hand orientation per hand position. As reconstruction of natural movements by use of three PCs is good (Fig. 8), this suggests that there are preferred hand orientations for any given catching position. While it is clear that there are manipulation tasks that involve rotational dexterity at a single hand position, for example, opening a jar, it is possible that the joint angle synergies underlying one-handed catching are important for many other reaching tasks as well.

It is worth mentioning that PCA only reduced dimensionality because variables were linearly correlated with each other, i.e., two or more joint angles changed in a temporally coordinated manner. One key aspect in the present study is the high number of analyzed DoFs and the broad scope of natural movement patterns. The fact that we consistently find three PCs that can efficiently describe such variable data is in line with our hypothesis that seemingly complex human arm movements, such as one-handed catching, may be described by target-dependent linear combinations of a small set of joint angle synergies. As linear combinations of these synergies can encode natural movements in a very compact manner, they may be part of the solution for the redundancy problem on the kinematic level of the human motor system.

4.1. Neural feedback, biomechanics, and muscle activation

Since our study focuses on the coupling of kinematic degrees of freedom, it emphasizes the behavioral aspect of spatially continuous, goal-directed movements rather than physiological aspects of muscle activation patterns or biomechanical properties of the upper limb. The consistent detection of three joint angle synergies for unrestrained, one-handed catching movements potentially reflects an invariant feature of movement control in other reaching tasks. Therefore, we suspect that the linear correlation of joint angles detected by our PCA suggests the presence of neural coupling by means of neural coactivation of muscles actuating different joints. Of course, there are at least three further sources of coupling that are likely to contribute to the observed linear correlation of DoFs. First, neural feedback is known to play a critical role in the control of arm movement (Gordon, Ghilardi, & Ghez, 1995; Graziano, 1999). Similarly, feedback control is likely to be beneficial to increase the reconstruction performance, especially in multiple-target-PCA. Secondly, muscle activation and de-activation functions that

transfer the time course of motoneuron activity into a time course of isometric muscle force are often modelled by first-order differential equations with separate time constants of force increase and decrease (Winter and Stark, 1988; Neptune and Hull, 1998; for review, see Zajac, 1989). Essentially, these models act as low-pass-filters with delayed force build-up/decline after a step onset/offset of motoneuron activity. For example, a de-activation time constant of 40 ms in elbow muscles (Winter and Stark, 1988) can cause an overlap of contraction time courses in elbow and proximal shoulder muscles within 40-50 ms in spite of lacking neural co-activation. Generally, muscle properties are known to contribute to kinematic properties of the human arm movements (Gribble & Ostry, 1996). Thirdly, interaction torques that are of purely mechanical origin occur necessarily in a moving multisegmented arm. Since all three of these mechanisms are of transient nature, they can hardly explain the entire scope of joint angle coupling detected by our PCA, mainly because this coupling is consistent across the entire workspace of catching movements. Interaction torques are known to be compensated for by the CNS (Gribble & Ostry, 1999), so part of the observed linear correlation is likely to be caused by this neural compensatory mechanism.

4.2. Single-target and multiple-target-PCA

A recent comparative study that evaluated the power of different methods for the extraction of movement synergies (Tresch, Cheung, & d'Avella, 2006) shows that PCA is capable of extracting synergies but exhibits lower performance than other methods. Nevertheless, our results show that PCA is sufficiently powerful to reduce dimensionality to the theoretical minimum of three effective DoFs. While it is possible that other methods could explain even more data variance with three DoFs, they couldn't possibly yield less than three DoFs. The main reason for us to apply PCA for identification of joint angle synergies was to determine an 'as-simple-as-possible' grouping of DoFs on the basis of consistent linear correlation. Since the minimum possible number of three PCs explains such a large amount of variance, these three PCs can serve as intuitive, plausible and potent description of synergies. Moreover, it suggests that a simple linear model can be used to explain a large fraction of the natural variability observed in one-handed catching.

Both single-target and multiple-target analyses clearly emphasize the target-dependent nature of the extracted PCs (Figs. 5, 7). Assuming that the inter-joint coupling captured by PCs reflects at least some aspects of the underlying neural controller, single-target and multiple-target analyses allow for two alternative interpretations, both of which involve a linear model that can serve as testable hypothesis in physiological studies.

Single-target-PCA yields PC sets, which are unique for each start-target-combination. Encoding movement in this manner seems hardly efficient at first sight, because each of these combinations would require a separate set of PCs. However, we also find that these sets tend to vary systematically over a large fraction of the arm's workspace (Fig. 5). Thus, the similarity of adjacent PC sets may be the result of target-dependent interpolation between a few cardinal sets of PCs that form the fundamental building blocks of one-handed catching movements. In the process of movement generation, these sets would have to be combined dynamically, in order to form a new target-dependent set of PCs.

In multiple-target-PCA, we extracted only one such cardinal set of PCs for all movements associated with one initial posture. Not surprisingly, because the postural basis for multiple-target-PCA is much broader, posture reconstruction based on 3 multiple-target PCs is less accurate but still good (Fig. 6). Our interpretation of this result is that different movements can be brought about by adjusting the weights of a single set of PCs, i.e., their scores, in a temporally coordinated fashion. Although we found different sets of PCs for each initial posture, it is conceivable that there is one single set of PCs that is even more general and could describe movements comprising arbitrary initial and target postures. The fact that both analyses produced a PC triplet with rather similar properties (Fig. 9) strongly supports the view that all recorded catching movements can be described by linear combination of a PC triplet.

4.3. Relation to neurophysiological evidence

Recent evidence from experiments on frogs suggests the existence of a small set of motor synergies that serve as distinct control modules in the spinal cord (d'Avella & Bizzi, 2005; d'Avella, Saltiel, & Bizzi, 2003). These studies analyze muscle activation, i.e., EMGs. Based on these EMGs, a set of motor primitives or basic muscle activation patterns is extracted. These time-varying synergies (d'Avella et al., 2003) are scaled in

amplitude, shifted in time and, eventually, linearly combined in order to form a variety of motor patterns.

In contrast to the approach taken by d'Avella et al., we have identified static joint-angle synergies, where the time course of movement depends on the time course of a corresponding set of scaling factors. In the case of human arm movements this posture-based approach is particularly plausible when considering posture-dependent tuning of motor cortex cells (Scott, Gribble, Graham, & Cabel, 2001; Scott & Kalaska, 1997). Further evidence for the importance of kinematic parameters in the generation of reaching movements was provided by direct stimulation of the motor cortex (Graziano, Aflalo, & Cooke, 2005; Graziano, Taylor, & Moore, 2002). These studies imply one-to-one mappings between workspace and arm posture located in the motor cortex. These mappings are robust against external disturbances and suggest joint angles or postures as a possible foundation.

Finally, joint angle synergies may serve as a kinematic template for models of interceptive arm movements in humans. Current modelling approaches for human catching movements favor feedback control over predictive open loop strategies (reviewed by Beek et al., 2003), in which time-varying synergies would not be required. Instead, the time-varying output of a feedback controller would drive the musculoskeletal system of the human arm and shoulder girdle. At this point, the triplets of joint angle synergies derived from our kinematic experiments may well serve as a starting point to model the correct degree of inter-joint coupling in unrestrained, one-handed catching movements.

Acknowledgments

We thank W.-J. Beyn and V. Thümmler for helpful comments on PCA and subspaces.

Current address of N. Troje: Dept. of Psychology, Queens University Kingston, Ontario, K7L 3N6, Canada

References

Alderson G. J. K., Sully, D. J., & Sully, H. G. (1974). An operational analysis of a one-handed catching task using high-speed photography. *Journal of Motor Behavior*, *6*, 217-226.

Atkeson, C. G., & Hollerbach, J. M. (1985). Kinematic features of unrestrained vertical arm movements. *The Journal of Neuroscience*, *5*, 2318-2330.

Beek, P. J., Dessing, J. C., Peper, C. E., & Bullock, D. (2003) Modelling the control of interceptive actions. *Philosophical Transactions of the Royal Society London Biological Sciences*, *358*, 1511-1523.

Bernstein, N. (1967). *The co-ordination and regulation of movements*. New York: Pergamon Press Ltd.

d'Avella, A., & Bizzi, E. (1998). Low dimensionality of supraspinally induced force fields. *Proceedings of the National Academy of Sciences of the United States of America*, *95*, 7711-7714.

d'Avella, A., & Bizzi, E. (2005). Shared and specific muscle synergies in natural motor behaviors. *Proceedings of the National Academy of Sciences of the United States of America*, *102*, 3076-3081.

d'Avella, A., Saltiel, P., & Bizzi, E. (2003). Combinations of muscle synergies in the construction of a natural motor behavior. *Nature Neuroscience*, *6*, 300-308.

Daffertshofer, A., Lamoth, C. J., Meijer, O. G., & Beek, P. J. (2004). PCA in studying coordination and variability: A tutorial. *Clinical Biomechanics*, *19*, 415-428.

Debicki, D. B., & Gribble, P. L. (2005). Persistence of inter-joint coupling during single-joint elbow flexions after shoulder fixation. *Experimental Brain Research*, *163*, 252-257.

Flash, T., & Hogan, N. (1985). The coordination of arm movements: an experimentally confirmed mathematical model. The Journal of Neuroscience, 5(7), 1688-1703.

Forner-Cordero, A., Levin, O., Li, Y., & Swinnen, S. P. (2005). Principal component analysis of complex multijoint coordinative movements. *Biological Cybernetics*, *93*, 63-78.

Galloway, J. C., & Koshland, G. F. (2002). General coordination of shoulder, elbow and wrist dynamics during multijoint arm movements. *Experimental Brain Research*, *142*, 163-180.

Georgopoulos, A. P. (1991). Higher order motor control. *Annual Review of Neuroscience*, *14*, 361-377.

Golub, G. H., & van Loan, C. F. (1989). *Matrix computations* (2nd ed.). Baltimore, MD: Johns Hopkins University Press.

Gomi, H., & Kawato, M. (1997). Human arm stiffness and equilibrium-point trajectory during multi-joint movement. *Biological Cybernetics*, *76*, 163-171

Gordon, J., Ghilardi, M. F., & Ghez, C. (1995). Impairments of reaching movements in patients without proprioception. I. Spatial errors. *Journal of Neurophysiology*, *73*, 347-360.

Gottlieb, G. L., Song, Q., Hong, D. A., Almeida, G. L., & Corcos, D. (1996). Coordinating movement at two joints: A principle of linear covariance. *Journal of Neurophysiology*, *75*, 1760-1764.

Graziano, M. S. (1999). Where is my arm? The relative role of vision and proprioception in the neuronal representation of limb position. *Proceedings of the National Academy of Sciences of the United States of America*, *96*, 10418-10421.

Graziano, M. S., Aflalo, T. N., & Cooke, D. F. (2005). Arm movements evoked by electrical stimulation in the motor cortex of monkeys. *Journal of Neurophysiology*, *94*, 4209-4223.

Graziano, M. S., Taylor, C. S., & Moore, T. (2002). Complex movements evoked by microstimulation of precentral cortex. *Neuron*, *34*, 841-851.

Gribble, P. L., & Ostry, D. J. (1996). Origins of the power law relation between movement velocity and curvature: Modeling the effects of muscle mechanics and limb dynamics. *Journal of Neurophysiology*, *76*, 2853-2860.

Gribble, P. L., & Ostry, D. J. (1999). Compensation for interaction torques during single- and multijoint limb movement. *Journal of Neurophysiology*, *82*, 2310-2326.

Haruno, M., & Wolpert, D. M. (2005). Optimal control of redundant muscles in steptracking wrist movements. *Journal of Neurophysiology*, *94*, 4244-4255.

Jackson, D.A. (1993). Stopping rules in principal component analysis: A comparison of heuristical and statistical approaches. *Ecology*, *74*, 2204-2214.

Kalaska, J. F., & Crammond, D. J. (1992). Cerebral cortical mechanisms of reaching movements. *Science*, *255*, 1517-1523.

Latash, M. L., Aruin, A. S., & Shapiro, M. B. (1995). The relation between posture and movement: A study of a simple synergy in a two-joint task. Human Movement Science, *14*, 79-107.

Laurent, M., Montagne, G., & Savelsbergh, G. J. P. (1994). The control and coordination of one-handed catching – the effect of temporal constraints. Experimental Brain Research, *101*, 314-322.

Lee, W. A. (1984). Neuromotor synergies as a basis for coordinated intentional action. *Journal of Motor Behavior*, *16*, 135-170.

Levenberg, K. (1944). A method for the solution of certain nonlinear problems in least squares. *Quarterly of Applied Mathematics*, *2*, 164-168.

Macpherson, J. M. (1991). In D. R. Humphrey & H. J. Freund (Eds.), *Motor control: Concepts and issues* (pp. 33-47). New York: Wiley Press.

Manly, B. F. (2004). Multivariate statistical methods: a primer (3rd ed.): Chapman & Hall.

Marquardt, D. W. (1963). An algorithm for least-squares estimation of nonlinear parameters. *SIAM Journal on Applied Mathematics*, *11*, 431-441.

Mazyn, L. I. N., Montagne, G., Savelsbergh, G. J. P., & Lenoir, M. (2006) Reorganization of catching coordination under varying temporal constraints. *Motor Control*, *10*,143-159.

Montagne, G., Laurent, M., Durey, A., & Bootsma, R. J. (1999). Movement reversals in ball catching. *Experimental Brain Research*, *129*, 87-92.

Morasso, P. (1981). Spatial control of arm movements. *Experimental Brain Research*, *42*, 223-227.

Mussa-Ivaldi, F. A., Giszter, S. F., & Bizzi, E. (1994). Linear combinations of primitives in vertebrate motor control. *Proceedings of the National Academy of Sciences of the United States of America*, *91*, 7534-7538.

Neptune, R. R. & Hull, M. L. (1998). Evaluation of performance criteria for simulation of submaximal steady-state cycling using a forward dynamic model. *Journal of Biomechanical Engineering*, *120*, 334-341.

Peper, C. E., Bootsma, R. J., Mestre, D., & Bakker, F. C. (1994). Catching balls: How to get the hand to the right place at the right time. *Journal of Experimental Psychology: Human Perception and Performance*, *20*, 591-612.

Post, A. A., Daffertshofer, A., & Beek, P. J. (2000). Principal components in three-ball cascade juggling. *Biological Cybernetics*, *82*, 143-152.

Sabatini, A. M. (2002). Identification of neuromuscular synergies in natural upper-arm movements. *Biological Cybernetics*, *86*, 253-262.

Sanger, T. D. (2000). Human arm movements described by a low-dimensional superposition of principal components. *The Journal of Neuroscience*, *20*, 1066-1072.

Santello, M., Flanders, M., & Soechting, J. F. (1998). Postural hand synergies for tool use. *The Journal of Neuroscience*, *18*, 10105-10115.

Scott, S. H., Gribble, P. L., Graham, K. M., & Cabel, D. W. (2001). Dissociation between hand motion and population vectors from neural activity in motor cortex. *Nature*, *413*, 161-165.

Scott, S. H., & Kalaska, J. F. (1997). Reaching movements with similar hand paths but different arm orientations. I. Activity of individual cells in motor cortex. *Journal of Neurophysiology*, *77*, 826-852.

Soechting, J. F., & Lacquaniti, F. (1981). Invariant characteristics of a pointing movement in man. *The Journal of Neuroscience*, *1*, 710-720.

Thomas, J. S., Corcos, D. M., & Hasan, Z. (2005). Kinematic and kinetic constraints on arm, trunk, and leg segments in target-reaching movements. *Journal of Neurophysiology*, *93*, 352-364.

Ting, L. H., & McKay, J. L. (2007). Neuromechanics of muscle synergies for posture and movement. *Current Opinion in Neurobiology*, *17*, 622-628.

Tresch, M. C., Cheung, V. C., & d'Avella, A. (2006). Matrix factorization algorithms for the identification of muscle synergies: Evaluation on simulated and experimental data sets. *Journal of Neurophysiology*, *95*, 2199-2212.

Troje, N. F. (2002). Decomposing biological motion: A framework for analysis and synthesis of human gait patterns. *Journal of Vision*, *2*, 371-387.

Winters, J. M., & Stark, L. (1988). Estimated mechanical properties of synergistic muscles involved in movements of a variety of human joints. *Journal of Biomechanics*, *21*, 107-1041.

Wolpert, D. M., & Ghahramani, Z. (2000). Computational principles of movement neuroscience. *Nature Neuroscience*, *3 Suppl.*, 1212-1217.

Yang, N., Zhang, M., Huang, C., & Jin, D. (2002) Synergic analysis of upper limb target-reaching movements. *Journal of Biomechanics*, *35*, 739-746.

Zajac, F. E. (1989). Muscle and tendon: Properties, models, scaling, and application to biomechanics and motor control. *Critical Reviews of Biomedical Engineering*, *17*, 359-411.

Figure and table legends

Fig. 1. Basic experimental setup. (a) Participants are instructed to catch an approaching ball. The ball is launched onto different trajectories traversing the workspace of the participant's right arm. Arm movements occur in 3D and are unconstrained. (b) Target positions. Sixteen different trajectories are brought about by varying the position and the angle of the shooting device. Idealized target positions are indicated by grey circles.

Fig. 2. Kinematic model. The arm is modeled as a kinematic chain consisting of 4 segments (a-d) with a total of 10 DoFs and 13 motion capture markers attached to it (m1 to m13). DoFs are illustrated by rotation axes. Joints are denoted by black circles. M1 represents a marker and the root joint of the kinematic chain. Markers m3 (attached to the 7th cervical vertebra), m4 (attached to the 10th thoracic vertebra), and m7 (attached to the scapula) are occluded by the body.

Fig. 3. Hand trajectories of participant CL. The X-Z-plane corresponds to the frontal plane of the participant. The ball is launched towards the participant from the direction of the positive part of the Y-axis. Catching positions are indicated by ellipsoids, the dimensions of which correspond to the standard deviation of the end points' distribution and are numbered according to Fig. 1b. (a) Hand trajectories originating from initial position 1. (b) Trajectories originating from initial position 2.

Fig. 4. Twenty-six three PCs explain most of the variance. PCA has been applied to all mean trials per start-target combination and person (single-target-PCA). Results have been averaged over participants (n = 9). Values above bars indicate cumulative percentage of explained variance of the first three PCs. Columns and error bars show means and std. across participants. (a) Results for mean trials of initial position 1. (b) Results for mean trials of initial position 2.

Fig. 5. PC sets vary consistently across the workspace. We compared subspaces spanned by sets of the first three PCs associated with five different target positions. (a) Compared target positions form a horizontal transect across the arm’s workspace and

comprise positions 2, 6, 10, 13, and 15. (b) Compared target positions form a vertical transect across the arm's workspace and comprise positions 5 to 8. In both transects, movements differ gradually from one target position to its neighboring positions. Here 3D subspaces within the 10D postural space are compared by computing the angle between two subspaces. The smaller the angle between the two subspaces, the more similar they are. Random 3D subspaces would result in an average angle of approximately 81° (dashed line). Adjacent columns show the angles between all 5 x 4 (Fig. 5a) and 4 x 3 (Fig. 5b) subspaces within the horizontal and vertical transect respectively. Columns and error bars show mean and SD among participants (n = 9).

Fig. 6. Results of multiple-target-PCA. Two sets of PCs per person were extracted. Left columns show results for multiple-target-PCA associated with initial position 1, right columns show results associated with initial position 2. Although here the first three PCs account for less variance than in the single-target-PCA, the cumulative value is still high (75%-80%). The second and third PC play a larger role than in single-target-PCA.

Fig. 7. Representative time courses of the scores of the first three PCs for different target positions (participant CL). Each movement has a set of time courses of scores associated with it. The magnitude of these scores is represented by multiples of standard deviations of the original data. (a) Time courses of scores of five target positions which form a horizontal transect within the workspace of the arm. (b) Time courses of scores associated with four target positions which form a vertical transect. Same transect as in Fig. 5. Differences between movements often correspond to gradual changes in amplitude of the time course of one or two of the scores.

Fig. 8. Reconstructed angular time courses based on a set of three PCs. Representative trial with original (gray lines) and reconstructed data (dashed lines). Most angular time courses allow a very accurate reconstruction. Both of the forearm angles (ulna θ and ψ) and one of the hand angles (hand θ) are less accurate, but the characteristics of their respective time courses are preserved; unphysiological joint angles never occurred.

Fig. 9. Coupling strengths between different DoFs for three PCs obtained from four different computations. Here, coupling strength is the respective element in the 10D PC vector and is specified for each DoF separately. PC 1 has very similar features in all situations, whereas PC 2 and PC 3 show more pronounced differences.

Table 1. Explained variance of the first three PCs based on the results from bootstrapped multiple-target PCA. Each multiple-target dataset (1600 x 10 postures) was bootstrapped with a sample size of 100 for each one of 2 start positions (s1, s2) and 9 participants. Eigenvalues, i.e., explained variance, of the first three PCs are given in percent. Numbers in parentheses denote variances of eigenvalues in percent.

Supplementary figure legends

Supplementary Fig. S1: Single-target-PCA based on covariance matrices, i.e., data sets where joint angle ranges were not normalized to unit variance. Compare with Fig. 4 of the manuscript. Panels separate trials according to initial hand position (a: initial position 1; b: initial position 2). Without normalization, the joint angles with the broadest ranges dominate the analysis. As a result, two PCs are sufficient to capture at least 97% of the data's variance. The third PC vanishes. This can be explained by the dominating effects of a few joint angles that essentially render the data sets of single start-target combinations two-dimensionally. This, however, does not happen when movements to more than one target are included (see Fig. S2).

Supplementary Fig. S2: Alternative analysis of multiple-target-PCA. Compare with Fig. 6 of the manuscript. (a) Multiple-target-PCA based on covariance matrices, i.e., data sets where joint angle ranges were not normalized to unit variance. Without normalization, the joint angles with the very largest ranges dominate the analysis, resulting in a larger fraction of variance explained by the first three PCs (more than 91%, compared to 78-91% in normalized data sets of Fig. 6). (b) Multiple-target-PCA based on correlation matrices, but using all single trials rather than averaged trials as done in Fig. 6). Depending on the participant, the number of single postures varied from 3358 to 5698 per PCA, as opposed to 1600 in Fig. 6. The result is very similar to that shown in Fig. 6; however the explained variance is slightly less (74-89%, compared to 78-91%). Both a)

and b) show that the choice of analysis does not change the number of significant PCs, i.e., the number of significant joint angle synergies.

Supplementary Fig. S3. Time course of PC scores based on 50 bootstrap PCAs. Original joint angle time courses are projected into the spaces spanned by the first three PCs of each bootstrap PCA. (a) Time courses of PC scores for catching movements toward three target positions located on a horizontal transect within the workspace of the arm. (b) Time courses of PC scores for catching movements toward four target positions located on a vertical transect. Same transect as in Fig. 5. The gaps between time courses for movements to different targets are often larger than the spread of the 50 bootstrap solutions, showing that there is a robust systematic dependence on target position.

Supplementary Fig. S4: Time course of individual joint angles after reconstruction of the original movement by use of the first three PCs. Compare with Fig. 8. Black traces show the reconstructed joint angle time courses for 50 bootstrap solutions of the PCA (calculated by use of the correlation matrix). Same bootstrap analyses as used for Fig. S3. Red traces show the corresponding original time courses as measured in the experiment. The spread of the reconstructed time courses is small, showing that the variability between trials of one participant has little effect on the reconstruction of joint angle time courses.

Supplementary Fig. S5: Loadings of the first three PCs (start position 1, participant CL, multiple-target-PCA). Black columns show the data from Fig. 9. White columns show the mean loadings of 15 sets of PCs calculated for noisy data sets. In each noisy data set, the marker positions were confounded by a random position offset. Standard deviation of the added noise was 8 mm. Note that this added noise was not equivalent to the estimated mean marker error of the original data set because here, noise was added independently for each marker and the resulting deviation from the kinematic chain could cumulate, whereas in the real experiments they could not do so. Arm postures and associated PCA were recalculated as in the original data set. Error bars show the standard deviation of the loadings. The mean noisy loadings differ from the original

loadings but the main features of the original PCs remain unaffected. Only one loading of PC 3, hand φ, reverses sign; however, the absolute value of this loading remains small. Standard deviations are small for PC 1 but increase for many loadings of PC 2 and PC 3 (but not all; see hand φ and θ of PC 2), indicating that these PCs are more strongly affected by noise than PC 1.

Supplementary videos

Files:

PC1_frontal_view.mpg

PC1_side_view.mpg

PC2_frontal_view.mpg

PC2_side_view.mpg

PC3_frontal_view.mpg

PC3_side_view.mpg

Each video shows the movement resulting from sinusoidal modulation of a single PC (PC 1, PC 2 and PC 3, respectively) around the average posture with maximum score amplitude set to three standard deviations. For each PC modulated in this way two views of the movement are provided, one from the frontal view and one from the right hand side view. See also Section 3.7 in the main text.

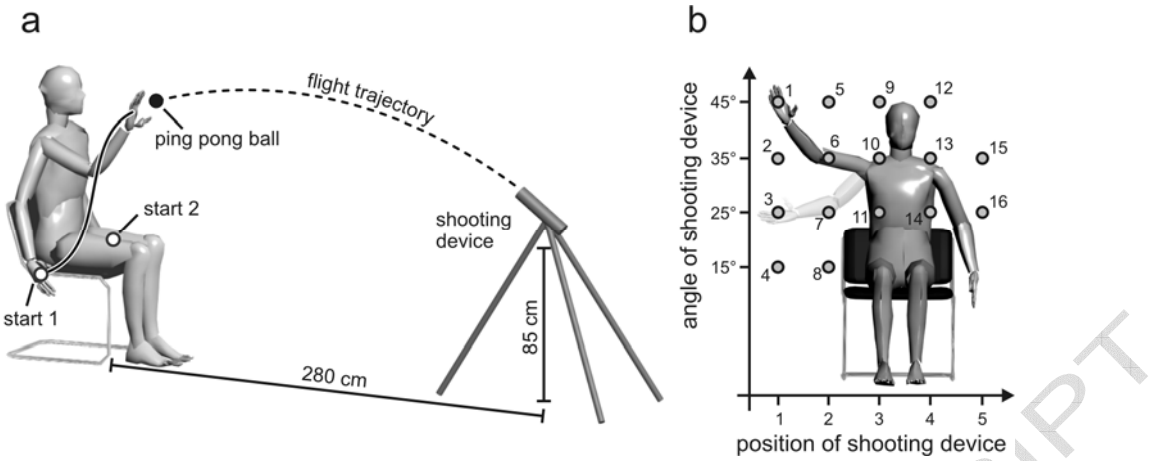

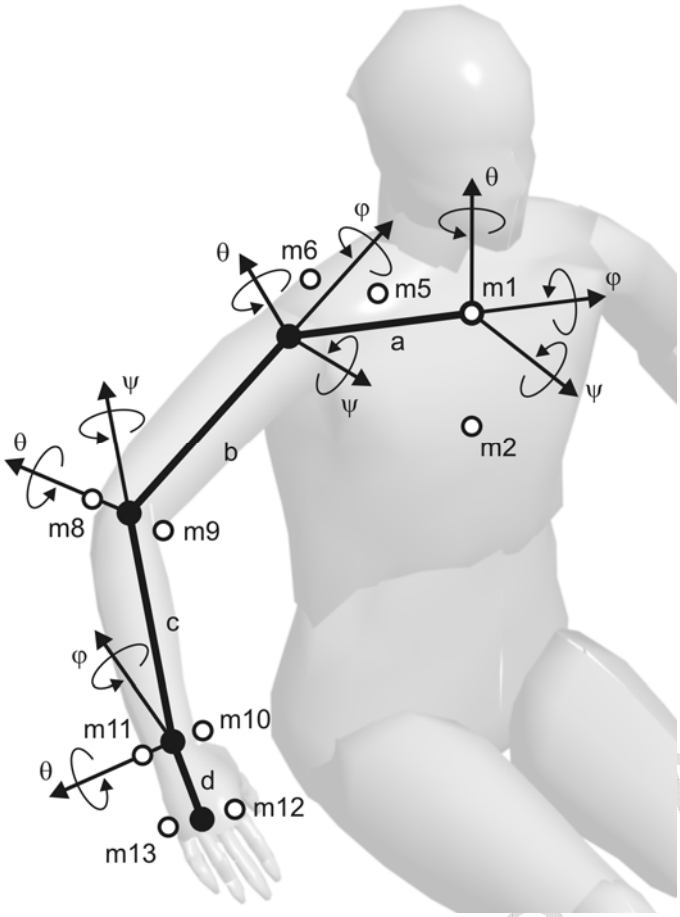

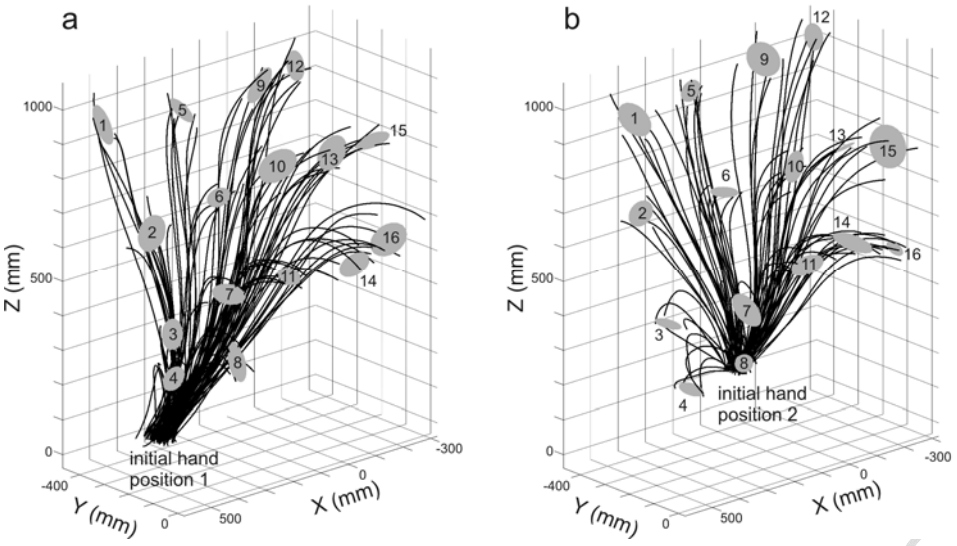

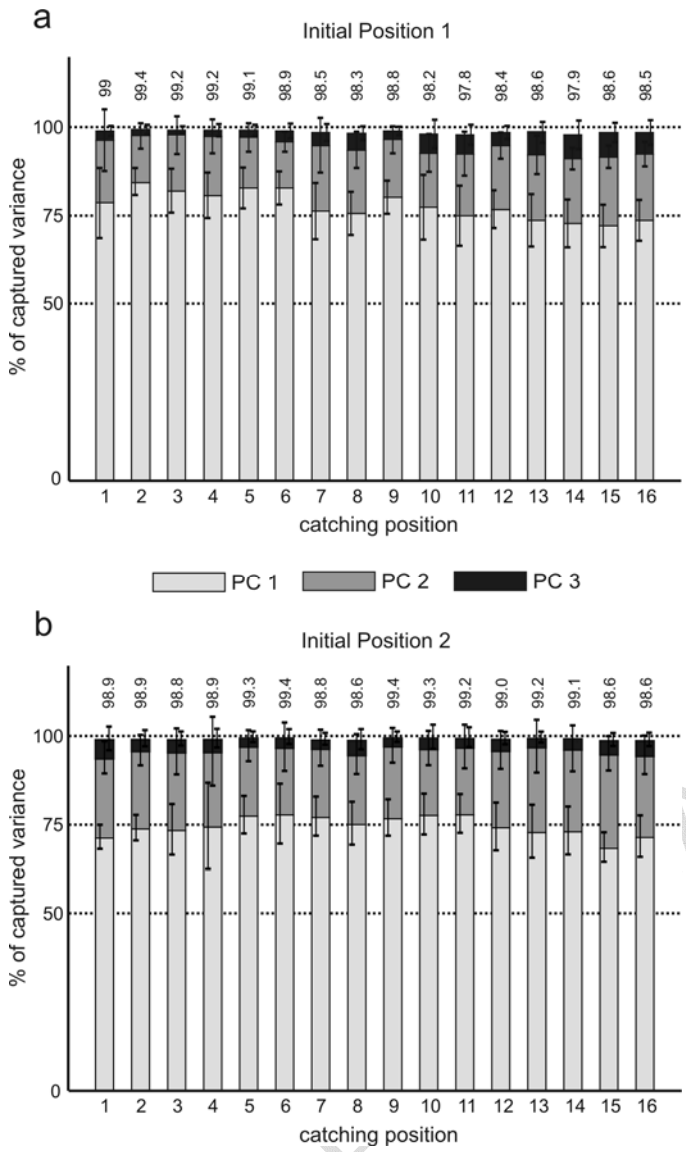

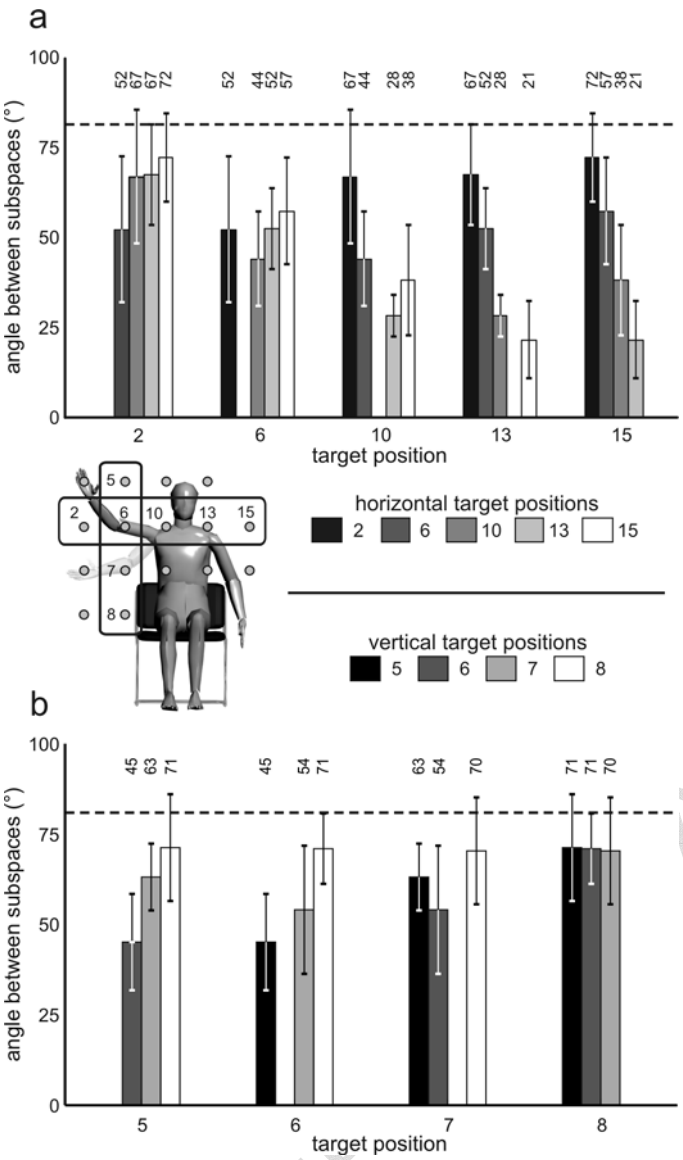

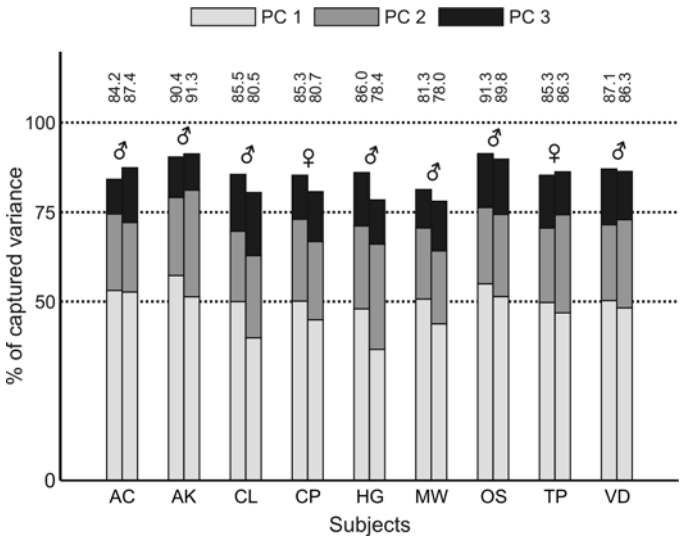

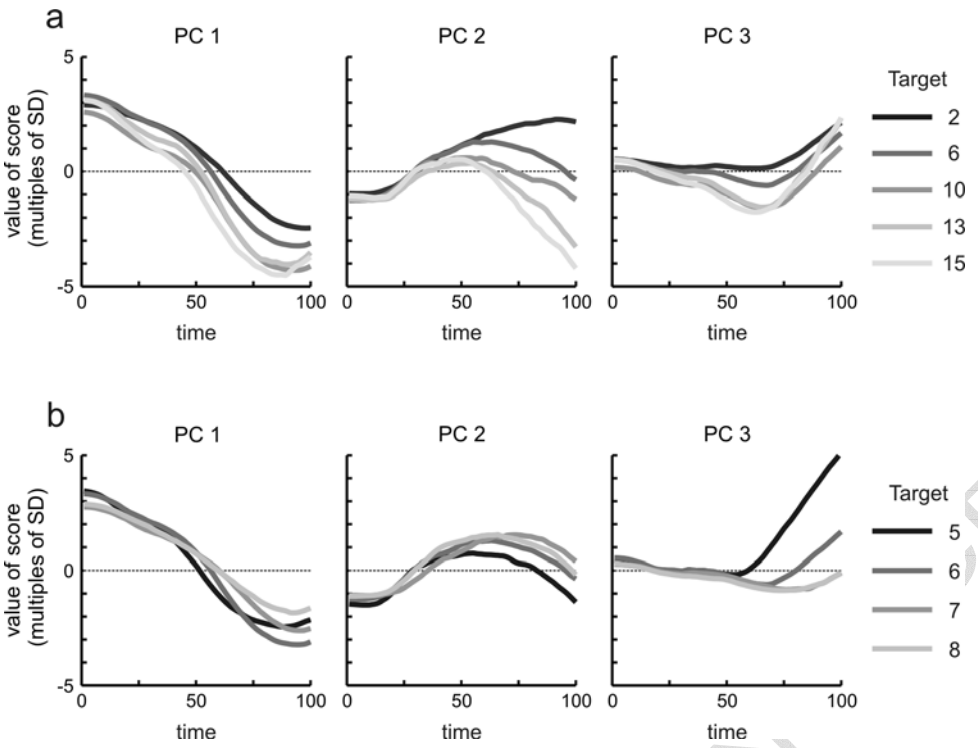

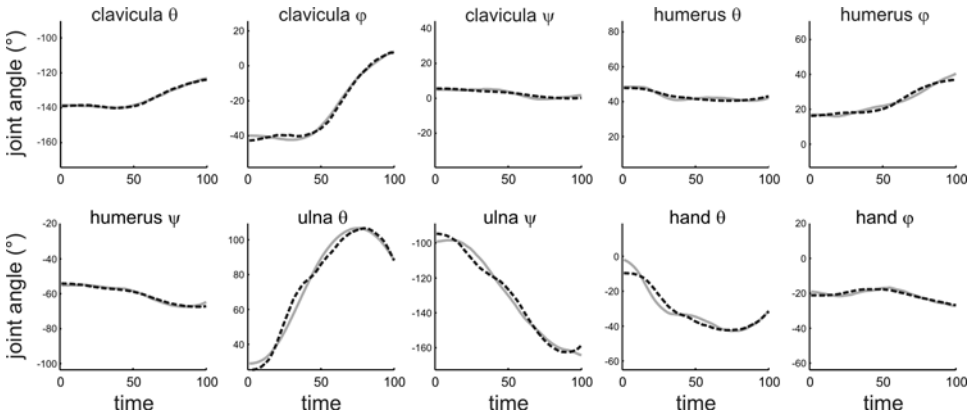

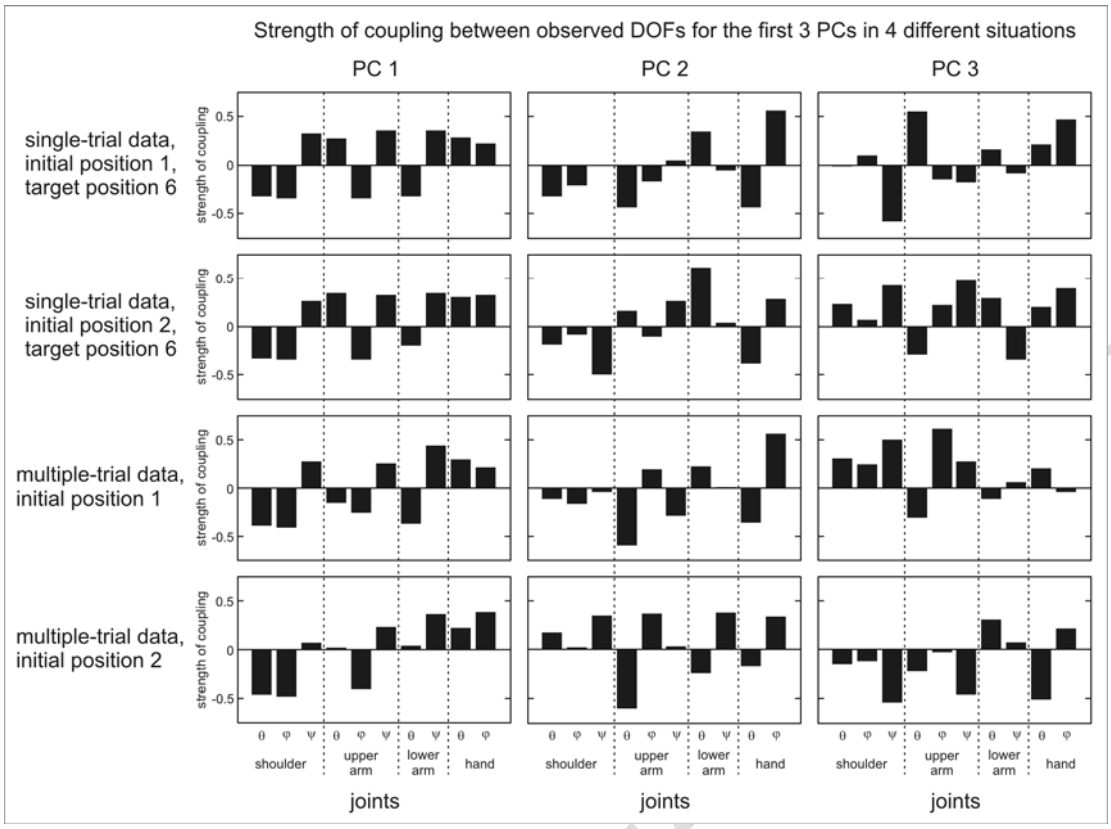

		AC	AK	CL	CP	HG	MW	OS	TP	VD	mean
PC 1	s1	53.4 % (0.34)	57.3 % (0.45)	50.1 % (0.54)	50.2 % (0.31)	48.1 % (0.21)	50.8 % (0.36)	54.9 % (0.57)	52.4 % (0.42)	49.7 % (0.51)	**51.9 %**
	s2	52.6 % (0.33)	51.3 % (0.18)	40.0 % (0.36)	45.0 % (0.60)	36.7 % (0.44)	43.8 % (0.26)	51.3 % (0.49)	46.9 % (0.37)	46.9 % (0.18)	**46.1 %**
PC 2	s1	21.2 % (0.36)	21.9 % (0.34)	19.6 % (0.22)	22.9 % (0.31)	23.1 % (0.26)	19.9 % (0.29)	21.4 % (0.30)	21.2 % (0.28)	20.8 % (0.36)	**21.3 %**
	s2	19.4 % (0.12)	29.8 % (0.29)	23.1 % (0.27)	21.8 % (0.50)	29.4 % (0.30)	20.5 % (0.17)	23.1 % (0.29)	22.8 % (0.24)	27.3 % (0.36)	**24.1 %**
PC 3	s1	9.8 % (0.28)	11.2 % (0.13)	11.9 % (0.43)	12.2 % (0.27)	14.9 % (0.16)	10.7 % (0.04)	15.1 % (0.15)	13.7 % (0.17)	14.8 % (0.10)	**12.7 %**
	s2	15.3 % (0.13)	10.2 % (0.19)	17.4 % (0.29)	13.9 % (0.24)	12.3 % (0.09)	13.9 % (0.06)	15.4 % (0.19)	14.1 % (0.34)	12.0 % (0.07)	**13.8 %**